Chapter 2

Combined Impact of Network Reconfiguration and Volt-VAR Control Devices on Energy Savings in Presence of Distributed Generation

2.1 Introduction

As discussed in previous chapter, utilities are paying renewed interest in the Volt-VAR control (VVC) techniques, due to their ability of energy savings and peak demand reduction [51] [52] [47] [53] [118] [119] [120] [121] [122]- [123]. On the other hand, distribution network reconfiguration (DNR) techniques have been used for reduction of losses, load balancing and service restoration [124] [29] [125] [126]- [127]. Therefore, it can be expected that a combined operation of Volt/VAR optimization (VVO) and DNR could be beneficial to distribution network operator (DNO) in both energy consumption and loss reduction.

To the best of knowledge of the authors, the combined impact of DNR and VVC devices on reduction of energy consumption has not been investigated so far. Besides, most of studies focused on real power demand alone, reactive power demand has been neglected,

but both active and reactive power demand varies with terminal voltage. Authors in [53] reveals that execution of VVC with reduced voltage does not guaranty reduction in system losses. In order to counter the above deficiencies, this chapter includes both real/reactive energy consumption and energy loss minimization in problem formulation. The impact of photovoltaic smart inverter (PVSI) on energy savings in distribution operation has also been studied. The main contributions of this chapter are as follows

- An efficient and optimal approach for coordinated operation of VVC, PVSI and DNR for energy demand reduction.
- Modified binary GWO (MBGWO) algorithm has been proposed for solution of optimization problem.
- Proposed method has been extended to include service restoration considering voltage regulation and peak demand saving under multiple faulty condition.
- Effect of different load models such as exponential and ZIP load model on energy demand reduction has been studied.
- The proposed method in association with photovoltaic smart inverter (PVSI) droop control has been employed to control the voltage violations under uncertain nature of PV generation during cloudy condition.
- Validation of proposed algorithm on both small scale (33 bus test system) and large scale (118 bus test system) distribution systems.

2.2 Functional smart Distribution Network

Energy demand reduction, healthy and mal-free operations are the main attributes of a smart distribution network (SDN). The schematic of the SDN has been illustrated in in Fig.2.1. It comprises of control centre, VVC devices (OLTC, VR & SCBs), remote controlled switches (RCS), PVSI and different load models connected through advanced distribution management system (ADMS). The ADMS have VVC and DNR functions for distribution operation and control.

In this chapter, a centralised as well as local control schemes have been proposed for optimal operation of distribution network such that no system constraints are violated.

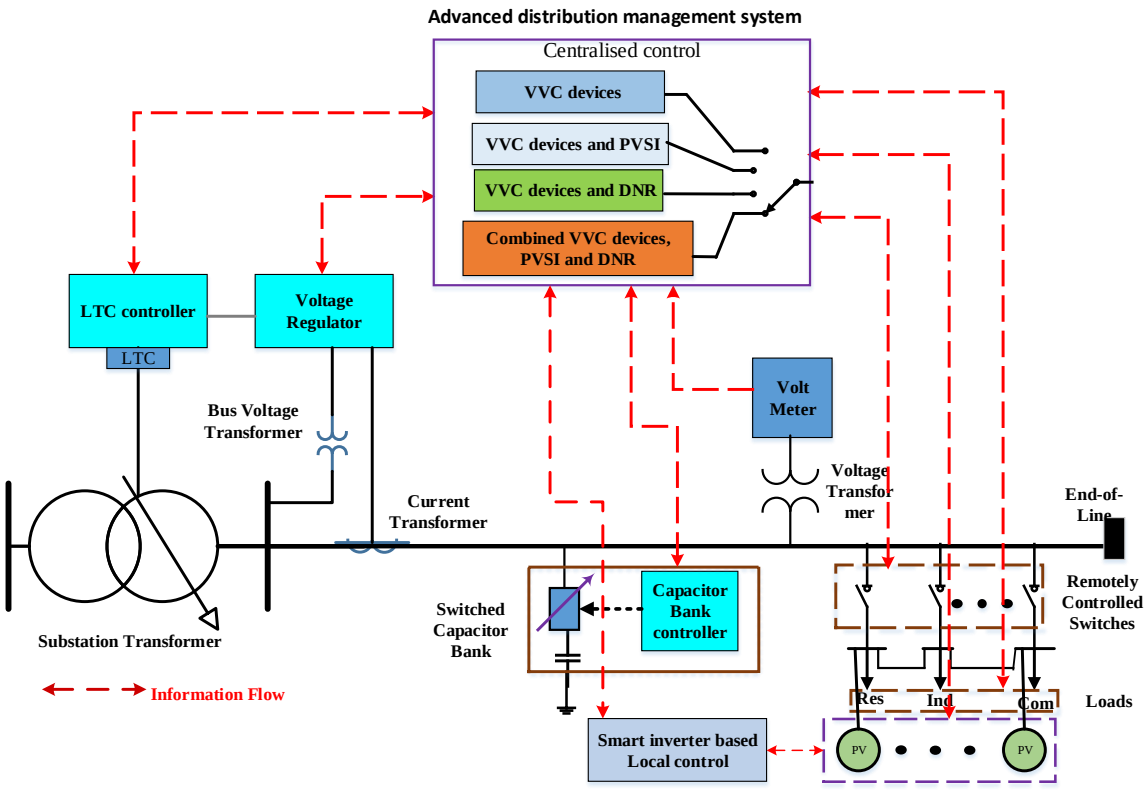

Figure 2.1: Schematic of smart distribution system

An efficient scheme for coordinated operation of VVC and DNR together has also been employed.

Centralized control provides the optimal set points for field devices in regular intervals based on measurements fed back through advanced metering infrastructure (AMI) and control sensors through communication infrastructures. It is assumed that communication and monitoring infrastructure function properly. However, local control action executed based on local measurements or the criterion adopted by the local operator.

2.3 Problem formulation

In present scenario, DNOs are more concerned towards the energy savings and assure the good power quality service to customers. In order to achieve this, the distribution control operational schemes such as VVC and DNR are required to be renewed to function in efficient manner. Apart from this, a local control action is much needed to avoid the voltage limit violations during PV power fluctuations. Considering these aspects, the problem has been formulated such that it covers the centralized as well as local control

with the objective of energy demand reduction without violating the regulation limits even in fluctuation in PV power. The objective function of this problem has been delineated as under.

2.3.1 Objective function

Energy demand of the distribution system is the sum of energy consumed by various consumers and energy losses of the system. Therefore, minimization of energy demand means savings in the energy consumption and energy losses. The objective function of the present investigation can be expressed by (2.1)

Minimize

$$E^S_{demand} = E^S_{cons.} + E^S_{loss.} \tag{2.1}$$

where

$$E^S_{cons.} = \sum_{t=1}^{T}\sum_{i=1}^{nd} \left| P^t_{cons.,i} + jQ^t_{cons.,i} \right| \tag{2.2}$$

$$E^S_{loss} = \sum_{t=1}^{T}\sum_{i=1}^{nd} \left| P^t_{loss,i} + jQ^t_{loss,i} \right| \tag{2.3}$$

here $P^t_{loss,i} = |I^t_i| \times R_i; Q^t_{loss,i} = |I^t_i| \times X_i$; where $|I^t_i| = \left(\frac{P^t_i + Q^t_i}{V^t_i}\right)^*$

Subjected to system constraints expressed by (2.4)-(2.14)

- Power balance constraints

$$P^t_{grid} - \sum_{i=1}^{nd} P^t_{cons.,i} - \sum_{i=1}^{nd} P^t_{loss,i} + \sum_{i\in spv} P^{inv,t}_{pv,i} = 0 \tag{2.4}$$

$$Q^t_{grid} - \sum_{i=1}^{nd} Q^t_{cons.,i} - \sum_{i=1}^{nd} Q^t_{loss,i} + \sum_{i\in spv} Q^{inv,t}_{pv,i} + \sum_{i\in scap} Q^{SCB,t}_i = 0 \Bigg\} \tag{2.5}$$

- Node Voltage constraints

$$V^{\min}_i \le V^t_i \le V^{\max}_i \tag{2.6}$$

- The OLTC transformer constraints

$$a^t = 1 + tap^t \frac{\Delta tap_{step}}{100} \tag{2.7}$$

here $tap^t \in \left\{tap^{\min}, ..., -1, 0, 1, ...tap^{\max}\right\}$

- SCB constraints

$$Q_i^{SCB,t} = st_i^t \Delta q_i^{cap}; i \in scap \tag{2.8}$$

Where, $st_i^t \in \{0, 1, ...st_i^{\max}\}$

- PVSI reactive power constraints

$$Q_{pv,i}^{inv,\max,t} = \sqrt{\left(S_{pv,i}^{inv,\max}\right)^2 - \left(P_{pv,i}^{inv,t}\right)^2}; i \in spv \tag{2.9}$$

$$-Q_{pv,i}^{inv,max} \leq Q_{pv,i}^{inv,t} \leq Q_{pv,i}^{inv,max} \tag{2.10}$$

- Radial structure constraint and number of switching operation of RCS

$$rank(\text{BBIM}) = nbr \tag{2.11}$$

$$N^S = \sum_{t=1}^{T} \sum_{m=1}^{nbr} \left| RCS_m^t - RCS_m^{(t-1)} \right| \tag{2.12}$$

- Maximum Load restoration constraint

$$\sum_{i \in sr} L_i^t = \sum_{i=1}^{nd} L_i^t \tag{2.13}$$

- Branch current constraints

$$I_m^t \leq I_m^{\max} \tag{2.14}$$

2.3.2 Load model

In this chapter, two load models have been considered, namely exponential load models (ELM) and polynomial load models (also known as ZIP load models). The mathematical representation of the these load models are given as follows

Exponential load models (ELM): active and reactive power consumption of the system is given as

$$P_{cons.i}^t = P_{cons.,i}^{n,t} \left(\frac{V_i^t}{V^n} \right)^{k_i^p} \tag{2.15}$$

$$Q_{cons.,i}^t = Q_{cons.,i}^{n,t} \left(\frac{V_i^t}{V^n} \right)^{k_i^q} \tag{2.16}$$

Polynomial load models (ZIP): active and reactive power consumption of the system is given as

$$P_{cons.i}^t = P_{cons.i}^{n,t} \left[Z_i^p \left(\frac{V_i^t}{V^n} \right)^2 + I_i^p \left(\frac{V_i^t}{V^n} \right) + P_i^p \right] \tag{2.17}$$

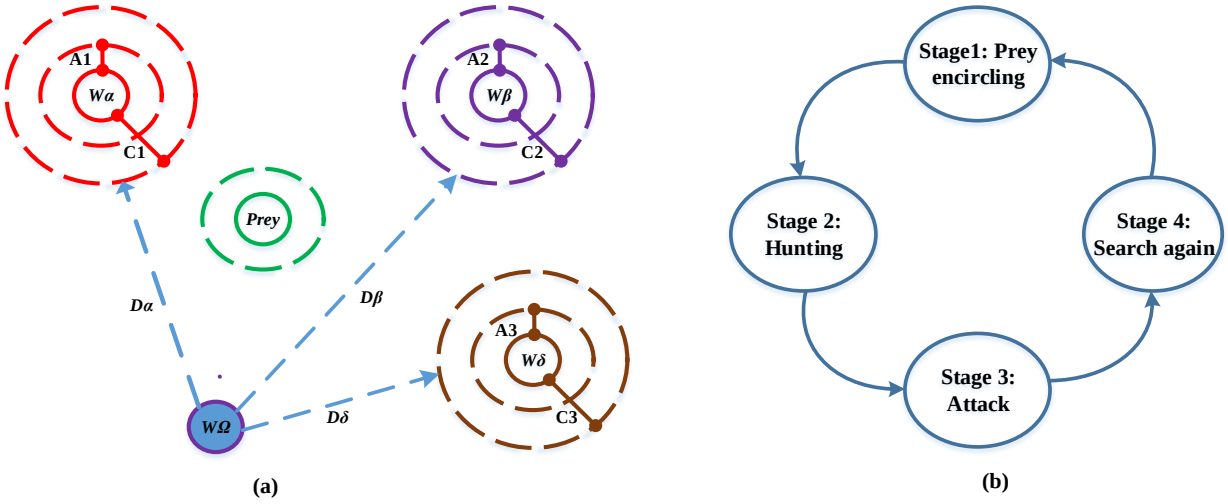

Figure 2.2: (a) Grey wolves in the search space, (b) Four stages of GWO algorithm

$$Q^{t}_{cons.i} = Q^{n,t}_{cons.i}\left[Z^{q}_{i}\left(\frac{V^{t}_{i}}{V^{n}}\right)^{2} + I^{q}_{i}\left(\frac{V^{t}_{i}}{V^{n}}\right) + P^{q}_{i}\right] \tag{2.18}$$

where, $Z^{p}_{i} + I^{p}_{i} + P^{p}_{i} = 1$ and $Z^{q}_{i} + I^{q}_{i} + P^{q}_{i} = 1$

2.4 Solution approach

Aforementioned problem formulation is given in (2.1)-(2.18) is a complex non-convex mixed integer non-linear optimization (MINLP) problem. In this chapter, A MBGWO algorithm has been proposed to solve the optimization problem.

2.4.1 Overview of GWO algorithm

GWO algorithm [128] simulates the leadership hierarchy of hunting mechanism of the grey wolf in the nature. Grey wolves in the search space can be visualized from Fig.2.2a where, grey wolves positions represent the potential solutions and location of the prey is the optimal solution. Grey wolves pack has four hierarchy level wolves: alpha, beta, delta and Omega wolves and their positions are W_{α}, W_{β}, W_{δ} and W_{Ω} respectively. For hunting the prey, four stages have to be applied as shown in Fig.2.2b.

1) *Stage of encircling the prey*: In this stage pack of grey wolves encircles a prey by repositioning individual agents according to the prey location as expressed in (2.19)

$$\overrightarrow{W}(iter+1) = \overrightarrow{W_{p}}(iter) - \overrightarrow{A}.\left|\overrightarrow{C}.\overrightarrow{W}_{p}(iter) - \overrightarrow{W}(iter)\right| \tag{2.19}$$

Where, *iter* is the current iteration, $\overrightarrow{W_p}$ is the prey position vector, $\overrightarrow{W}$ is the grey wolf position vector, $\overrightarrow{A} = 2a.\overrightarrow{r_1} - a$ and $\overrightarrow{C} = 2\overrightarrow{r_2}$ denotes coefficient vectors, a is exploration rate, which is linearly diminished from 2 to 0 over a course of iterations controlling exploration and exploitation, $\overrightarrow{r_1}\&\overrightarrow{r_2}$ are the random vectors in the range of [0,1].

2) *Stage of hunting the prey*: In this stage, hunting is performed by group of wolves based on the information coming from alpha, beta, and delta wolves, which are anticipated to know the prey location. This can mathematically be expresses as in (2.20)

$$\overrightarrow{W}(iter+1) = \left(\frac{\overrightarrow{W_1} + \overrightarrow{W_2} + \overrightarrow{W_3}}{3}\right) \tag{2.20}$$

Where $\overrightarrow{W_1}, \overrightarrow{W_2}, \overrightarrow{W_3}$ are defined as in equation ((2.21))

$$\left.\begin{aligned} \overrightarrow{W_1} &= \overrightarrow{W_\alpha} - \overrightarrow{A_1}.\left|\overrightarrow{C_1}.\overrightarrow{W_\alpha} - \overrightarrow{W}\right| \\ \overrightarrow{W_2} &= \overrightarrow{W_\beta} - \overrightarrow{A_2}.\left|\overrightarrow{C_2}.\overrightarrow{W_\beta} - \overrightarrow{W}\right| \\ \overrightarrow{W_3} &= \overrightarrow{W_\delta} - \overrightarrow{A_3}.\left|\overrightarrow{C_3}.\overrightarrow{W_\delta} - \overrightarrow{W}\right| \end{aligned}\right\} \tag{2.21}$$

Where $\overrightarrow{W_\alpha}, \overrightarrow{W_\beta}, \overrightarrow{W_\delta}$ are the first three best solutions at a given iteration *iter*, $\overrightarrow{A_1}, \overrightarrow{A_2}, \overrightarrow{A_3}$ are similar to $\overrightarrow{A}$, $\overrightarrow{C_1}, \overrightarrow{C_2}, \overrightarrow{C_3}$ are similar to $\overrightarrow{C}$.

3) *Stage of attacking the prey (exploitation)*: In this stage, wolves approach the prey, by decreasing the value of exploration rate a as given by (2.22)

$$a = 2 - iter.\frac{2}{iter^{max}} \tag{2.22}$$

Where, *iter* is the current iteration, $iter^{max}$ is maximum number of iterations.

4)*Stage of searching for prey (exploration)*: In this stage, if the prey location has not yet located, grey wolves depart from the group to search again for the prey. The wolf, which finds the better prey is called as new alpha wolf, remaining wolves are categorized as beta, delta and omega wolves according to the position with respect to the prey position.

2.4.2 Modified Binary Grey wolf optimization (MBGWO)

The conventional GWO (CGWO) algorithm has following limitations as given below

- It is designed for continuous search space, hence does not guarantee optimal solution for the integer problem.

- Due to its memory-less population characteristics, historical personal data can not be exploited by the next generation agents. Therefore, updated position has chance to get trapped in the local optimal because of lack of diversity among the agents.

In order to explore the information available at historical personal best and global best position to achieve better position, modified grey wolf position updating [129] is carried out using (2.23)-(2.26).

$$\overrightarrow{\chi}(iter+1) = \left\{ \begin{array}{l} w.\left(\frac{\overrightarrow{W_1}+\overrightarrow{W_2}+\overrightarrow{W_3}}{3}\right) \\ +k_1.r_2.\left(\overrightarrow{W_{pbest}} - \overrightarrow{W}\right) + k_2.r_3.\left(\overrightarrow{W_1} - \overrightarrow{W}\right) \end{array} \right\} \tag{2.23}$$

Where, r_1 and r_2 are the random vectors in [0,1]. k_1, k_2 denotes the individual and communication coefficient respectively. W_{pbest} represents the personal historical best position and w is the inertia weight, which is linearly decreased from initial ($w_{initial}$) value to final (w_{final}) value as given in (2.24)

$$w(iter) = \frac{iter_{max} - iter}{iter_{max}} \times (w_{initial} - w_{final}) + w_{final} \tag{2.24}$$

Wolf position updating mechanism as shown in (2.23), has been inspired by particle swarm optimisation (PSO) algorithm [130]. The first term on the right hand side (RHS) of the (2.23) represents the average positions of the first three best wolfs, which provides the necessary momentum for search agents across search space. Similar to PSO, the second term on RHS of (2.23) is known as "cognitive" component, which represents the personal thinking of each search agent, and move towards their own best position found so far. The third term on RHS of (2.23) is known as "social" component similar to PSO, which represents the collaborative effect of the search agents in determining the global optimal solution and pulls the search agents towards the global best position found so far.

In order to utilise for the discrete variable, a binary updated wolf position vector is given as

$$\overrightarrow{W}(iter+1) = \left\{ \begin{array}{ll} 1 & if sig(\overrightarrow{\chi}(iter+1)) \geq rand \\ 0 & otherwise \end{array} \right. \tag{2.25}$$

Where, $rand$ are the random number in [0,1], and sig is the sigmoid transformation function given by (2.26)

$$sig(\overrightarrow{\chi}(iter+1)) = \frac{1}{1+e^{-\overrightarrow{\chi}(iter+1)}} \tag{2.26}$$

Further, obtaining the radial topology of the distribution network is a difficult task since a very large number of infeasible individuals appear during initial stage and intermediate stages of the evolutionary process in CGWO. In order to solve this, a branch-node incidence matrix (BNIM) has been utilized. The dimension of the BNIM matrix is $nbrnd$, where nbr and nd are the number of branches and nodes in the network respectively. Elements of matrix can be finding out as under

$$BNIM_{ij} = \begin{cases} 1 & \text{if the } i\text{th branch is incident to and oriented away from the } j\text{th node} \\ -1 & \text{if the } i\text{th branch is incident to and oriented toward the } j\text{th node} \\ 0 & \text{if the } i\text{th branch is not incident to the } j\text{th node} \end{cases} \tag{2.27}$$

The matrix obtained from by deleting the column corresponding to the reference node in BNIM is the branch-bus incidence matrix (BBIM). The dimension of BBIM matrix is $nbr \times (nd-1)$ and the rank of BBIM matrix is $nd-1 = nbr$. BBIM matrix is a square matrix and its determinant is ± 1 , means that topology is radial structure but there is a chance of isolated buses in the network. In order to overcome it, rank of the matrix should be $(nd-1)$. In case of isolated buses present in the network, the rank will be smaller than $(nd-1)$. Fig.2.3 shows the flow chart representation for obtaining the radial topology using BBIM.

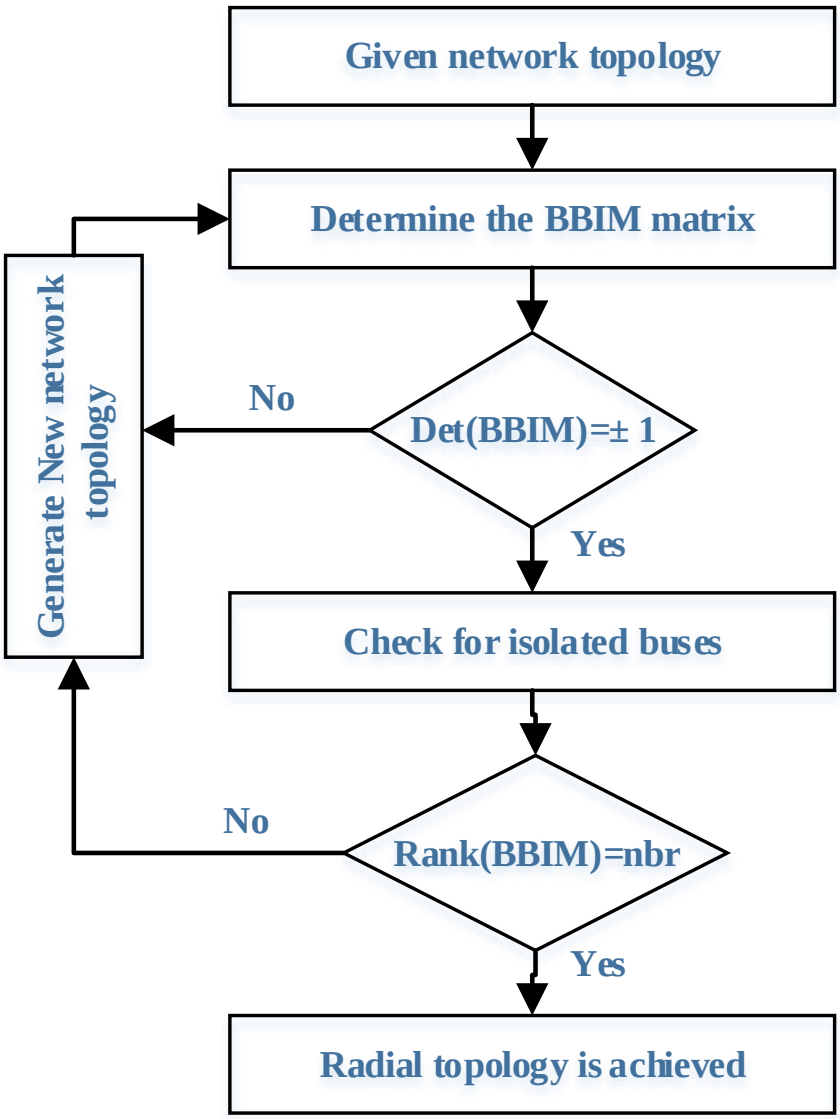

Figure 2.3: Flow chart to achieve radial topology using BNIM technique

2.4.3 Implementation of MBGWO algorithm on reduction of energy demand

In this section, proposed MBGWO employed as a centralised control algorithm, which is described above sub section 2.4.1 and 2.4.2. Implementation of MBGWO algorithm on reduction of energy demand is given in Algorithm 1.

Algorithm 1 MBGWO algorithm for energy demand reduction

Input: feed the distribution system data, set the MBGWO parameters such as population size (N_w) and maximum number of iterations ($iter^{max}$), k_1,k_2 coefficients, $w_{initial}$ & w_{final} as given Appendix A.1
divide the agent dimensions to accommodate the control variables (tap position of OLTC transformer, steps of SCBs, reactive power compensated from PVSI and status of remote controlled switches)
repeat
    initialise N_w agents randomly within allowable limit to construct a population
    check for radial topology of the distribution network using BBIM technique [126]. If YES goto 6, otherwise re-initialized population, then follow 5.
    conduct power flow analysis and evaluate the value of fitness function corresponding to each agent using (2.1) and find the W_α, W_β, and W_δ
    while $iter \leq iter^{max}$ **do**
        for each agent **do**
            update current agent position using (2.25)
        end for
        update the values of a, A, and C.
        evaluate the value of fitness function using (2.1)
        if system constraints (2.4) to (2.14) are satisfied **then**
            update the W_α, W_β, and W_δ
        else
            discard the result
        end if
    end while
    terminate iterative process and accept final wolf position as solution. Accept the settings of control devices
until t=T
Output: energy demand reduction over a specific time (T)

2.4.4 Implementation of MBGWO algorithm for service restoration

In this section, MBGWO algorithm has been employed for service restoration considering voltage regulation and peak demand reduction under faulty condition. For fast load restoration, heuristic rules [29] has been incorporated in the optimization algorithm. Proposed algorithm for service restoration considering voltage regulation and peak demand reduction has been described in Algorithm 2.

Algorithm 2 MBGWO algorithm for service restoration

1: **Input**: read the system data and fault location, set the MBGWO parameters such as population size (N_w) and maximum number of iterations ($iter^{max}$), k_1,k_2 coefficients, $w_{initial}$ & w_{final} as given Appendix A.1
2: divide the agent dimensions to accommodate the control variables (tap position of OLTC transformer, steps of SCBs, and reactive power compensated from PVSI)
3: apply heuristics rules [29] for service restoration via DNR
4: evaluate the values of fitness function corresponding to each agent using (2.1) and find the $\overrightarrow{W_\alpha}, \overrightarrow{W_\beta}$, and $\overrightarrow{W_\delta}$
5: **while** $iter \leq iter^{max}$ **do**
6: **for** each agent **do**
7: update current agent position using (2.25)
8: **end for**
9: update the values of a, A, and C.
10: apply heuristics rules for service restoration via DNR
11: evaluate the value of fitness function using (2.1)
12: **if** system constraints (2.4) to (2.14) are satisfied **then**
13: update the $\overrightarrow{W_\alpha}, \overrightarrow{W_\beta}$, and $\overrightarrow{W_\delta}$
14: **else**
15: discard the result
16: **end if**
17: **end while**
18: terminate iterative process and accept final wolf position as solution.
19: **output**: accept the final radial network and settings of VVC devices and PVSI reactive power

2.4.5 Implementation of MBGWO algorithm under sudden variation of generation/load

The distribution system will operate optimally and efficiently through set control points determined by MBGWO algorithm. However, voltage violations may occurs within defined VVC operation due to various reasons such as sudden variation of generation/ load. Therefore, to resolve this problem the proposed control algorithm with local smart inverter control has been utilised. The Volt/VAR droop characteristics used in present study has been shown in Fig.2.4. It is piecewise linear to the voltage following a path passing through the four points A_1, A_2, A_3 and A_4. The range between points A_2 and A_3 is defined as dead band range where, inverter neither absorbs nor injects the VAR . Before the point A_2 , inverter can inject the reactive power to the grid till point A_1 is reached. Before point A_1, inverter can inject the available maximum reactive power. However, when the voltage is above point A_3 , inverter absorbs reactive power from the grid till point A_4 is reached. After point A_4, inverter absorbs the available maximum reactive power. The compensated reactive power at any instant, t is determined using (2.28).

$$Q_{pv,i}^{inv,t}\left(V_i^t\right) = \begin{cases} Q_{pv,i}^{inv,\max} & V_i^t < V_1^{A_1} \\ \frac{V_i^t - V_2^{A_2}}{V_1^{A_1} - V_2^{A_2}} Q_{pv,i}^{inv,\max} & V_1^{A_1} \leq V_i^t < V_2^{A_2} \\ 0 & V_2^{A_2} \leq V_i^t \leq V_3^{A_3} \\ -\frac{V_i^t - V_3^{A_3}}{V_4^{A_4} - V_3^{A_3}} Q_{pv,i}^{inv,\max} & V_3^{A_3} < V_i^t \leq V_4^{A_4} \\ -Q_{pv,i}^{inv,\max} & V_i^t > V_4^{A_4} \end{cases} \tag{2.28}$$

Proposed MBGWO algorithm in conjunction with PVSI droop scheme in order to control the voltage during cloudy condition has been described in Algorithm 3.

2.5 Simulation results and discussions

In this section the proposed control algorithms have been validated through simulation results followed by discussion. The proposed control algorithm has been implemented on MATLAB environment, run on a computer with a Core i3 2.5GHz processor and 4 GB RAM.

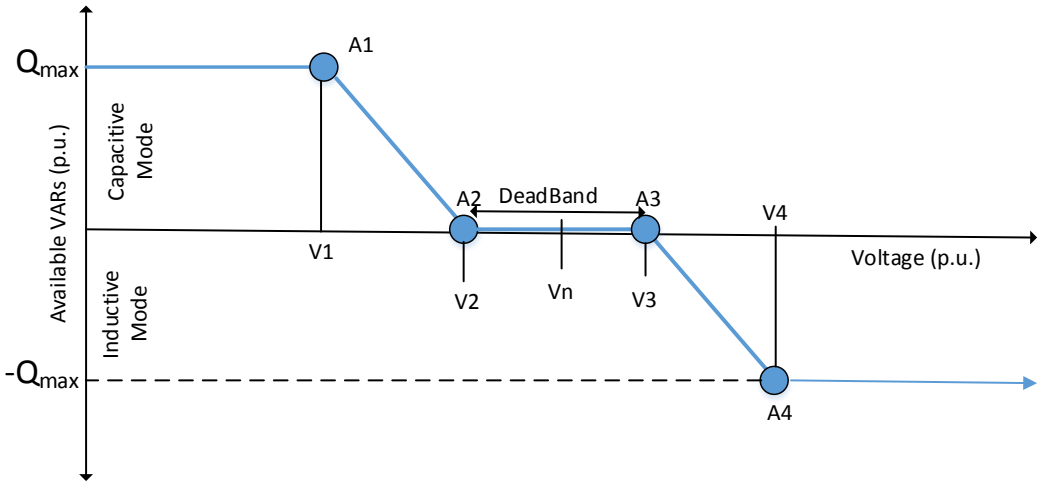

Figure 2.4: Volt/VAR droop characteristics

Algorithm 3 MBGWO algorithm with conjunction of PVSI droop control

Input: feed the settings of VVC devices, PVSI reactive power and status of RCS as obtained in **Algorithm 1**. Set the droop controller parameters (A_1, A_2, A_3 and A_4)
monitor the lowest voltage of the network, then verify the monitored voltage limits
if $V_2^{A_2} \leq V_i^t \leq V_3^{A_3}$ **then**
    remain the active and reactive power dispatch of PVSI as determined in **Algorithm 1**
else if $V_i^t < V_2^{A_2}$ **then**
    PVSI droop controller operates in capacitive region.
    PVSI injects the reactive power as governed by (2.28)
else$V_i^t > V_3^{A_3}$
    PVSI droop controller operates in inductive region.
    PVSI absorbs the reactive power as governed by (2.28)
end if
if voltage is still violates the permissible limits **then**
    reschedule the settings of VVC devices, PVSI reactive power and status of RCS by using **Algorithm 1**
else
    remain same as previous settings
end if
Output: desired settings of control parameters have been achieved

2.5.1 Test systems description

The performance of the algorithm has been tested on two test systems

- *Test system 1(TS-1):* 33 bus distribution system [131]
- *Test system 2(TS-2):* 118 bus distribution system [132]

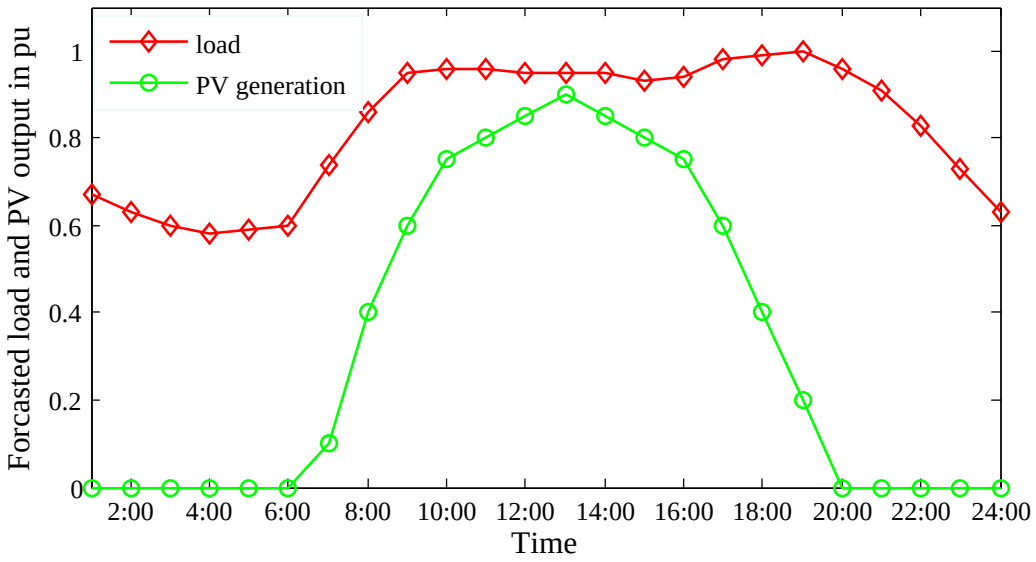

Figure 2.5: Typical load and PV generation in per unit

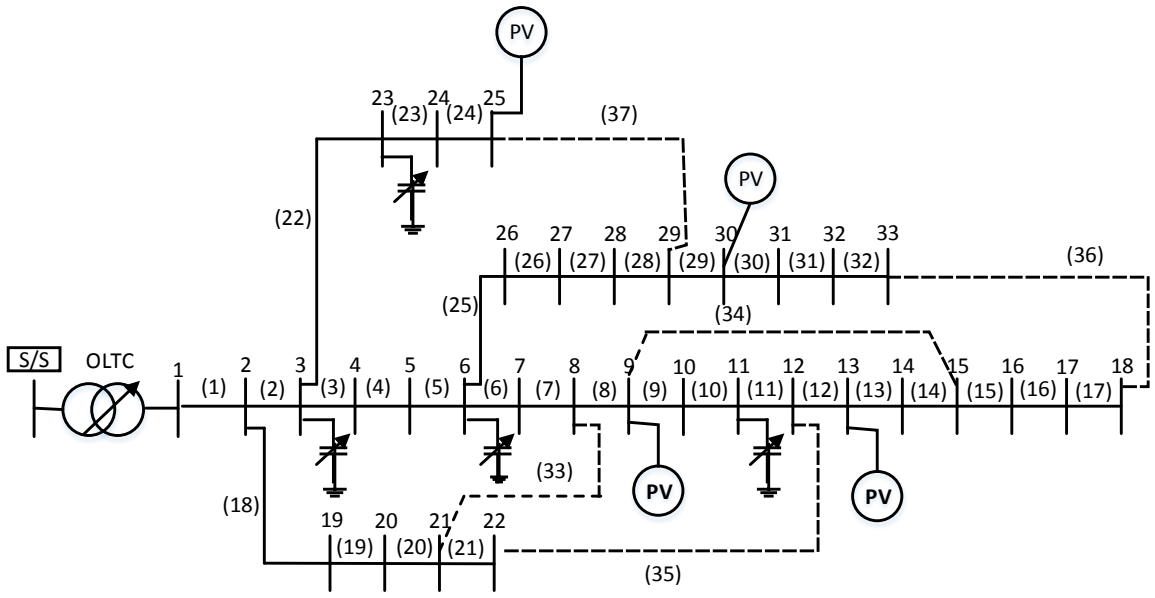

Figure 2.6: modified 33 bus distribution system (TS-1)

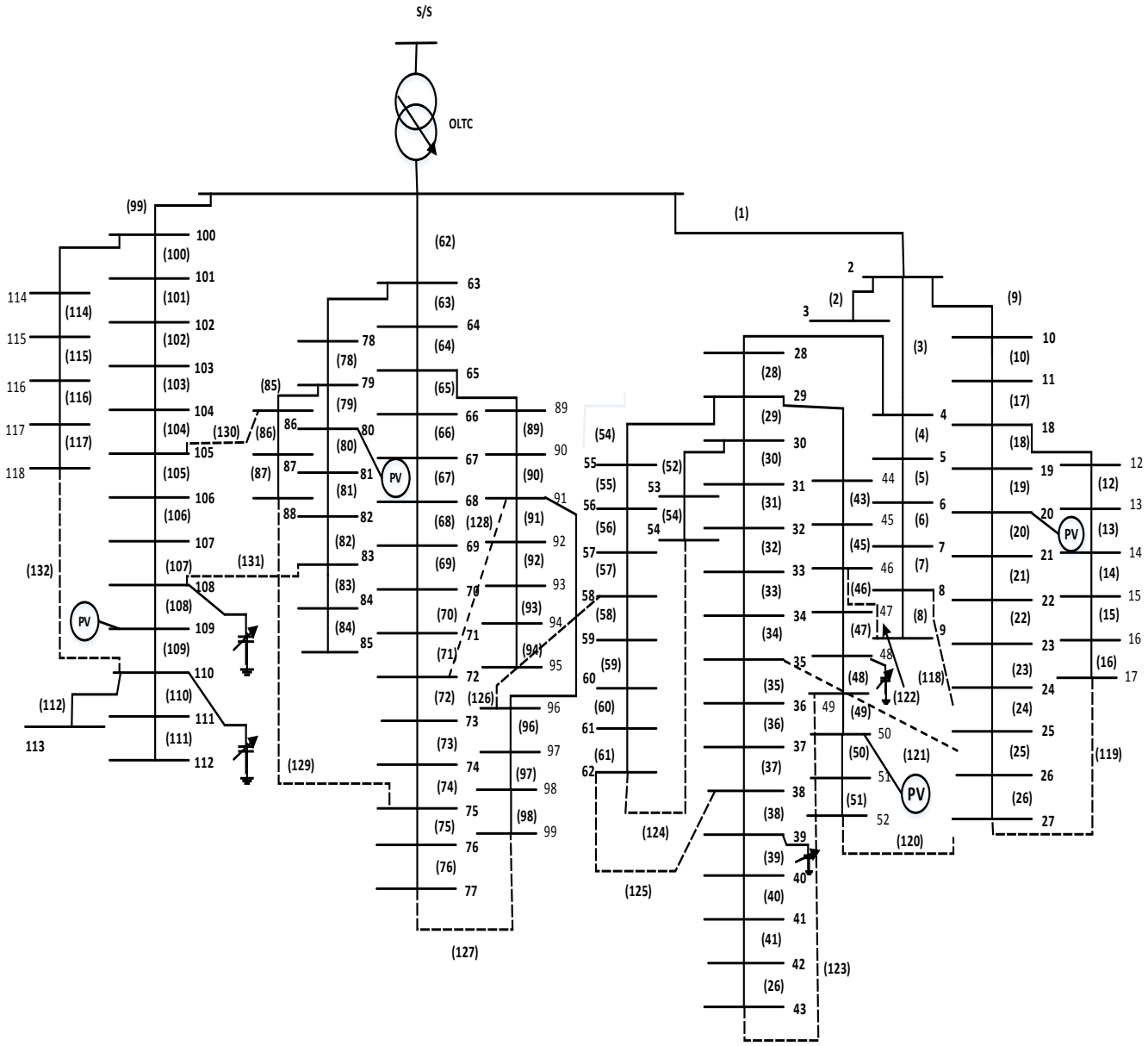

Figure 2.7: modified 118 bus distribution system (TS-2)

Single line diagram of TS-1 and TS-2 have been shown in Fig.2.6 and Fig.2.7 respectively. For both TS, it is assumed that OLTC transformer is connected between substation and node 1. Table 2.1 depicts the detailed information of both TS. Exponential and ZIP load model coefficients of different customers (industrial, residential and commercial) have been taken from [120] and [133] respectively. The typical load and PV active power generation in per unit for period of 24 hours have been shown in Fig.2.5.

Table 2.1: Test system information

Parameters	TS-1	TS-2
Nominal voltage (kV)	12.66	11
Nominal active power demand (MW)	3.715	22.71
Nominal reactive power demand (MVAR)	2.3	17.04
SCBs installed locations	3, 6, 11, 23	39, 48, 108,110
each SCB capacity(kVAR)	two sets of 150	four sets of 150
PVSI installed locations	PV1@9, PV2@13, PV3@25, PV4@30	PV1@20, PV2@50, PV3@80, PV4@110
Each PVSI capacity (MVA)	0.280	1.000
initial position of four SCBs	{0,0,0,0}	{0,0,0,0}
initial opened RCS	{Branch (33)-(37)}	{Branch (118)-(132)}
Industrial loads	Bus 1-4	Bus 1-10
Residential loads	Bus 5-18, Bus 29-33	Bus 11-68,Bus 78-108
Commercial loads	Bus 19-28	Bus 69-77,Bus 109-118
permissible voltage limits	0.95-1.05 pu	0.95-1.05 pu

Table 2.2: Four scenarios

Scenarios	VVC devices	PVSI	DNR
Scenario 1 (SC-1), method in [36]	✓	✗	✗
Scenario 2 (SC-2), method in [53]	✓	✓	✗
Scenario 3 (SC-3), method in [127]	✓	✗	✓
Scenario 4 (SC-4), proposed method	✓	✓	✓

✗- indicates not considered, ✓- indicates considered

2.5.2 Validation of centralized control using proposed MBGWO algorithm for energy demand reduction

In order to examine the performance the centralised algorithm using proposed MBGWO algorithm, four scenarios have been considered, as depicted in Table 2.2. The table represents the various combination of control parameters such as VVC devices, PVSI and DNR operations to reduce the energy demand in each scenario by optimally setting their control parameters.

The simulation results of both TS under four scenarios have been tabulated in Table 2.3. It is to be mentioned that energy terms such as energy demand, consumption and losses for four scenarios have been compared with traditional VVC (TVVC) method [53] for exponential load model (ELM) over a specific day.

2.5.2.1 Scenario 1

Under this scenario, it is assumed that PVSI is operated at unity power factor mode, whereas network topology is fixed as initial, OLTC taps and SCBs operation remains active. E^S_{demand} reduction obtained by optimal coordination of VVC devices compared to TVVC technique has been discussed for TS-1 and TS-2 as under

(a)TS-1: E^S_{demand} has been reduced by 4.53%. $E^P_{cons.}$ and $E^Q_{cons.}$ have been reduced by 2.866% and 9.68% respectively. E^P_{loss} and E^Q_{loss} are remain same as TVVC method.

(b) TS-2: E^S_{demand} has been reduced by 4.42%. $E^P_{cons.}$ and $E^Q_{cons.}$ have been reduced by 2.58% and 7.66% respectively. E^P_{loss} and E^Q_{loss} have been reduced by 1.73% and 1% respectively.

Thus, under scenario 1, optimal VVC scheme is capable to reduce the E^S_{demand} upto 4.53% and 4.42% in TS-1 and TS-2 respectively.

2.5.2.2 Scenario 2

Under this scenario, it is assumed that network topology is fixed at initial, whereas PVSI is operated at Volt-VAR control mode, OLTC taps and SCBs operation remains active.

(a)TS-1: E^S_{demand} has been reduced by 5.32%. $E^P_{cons.}$ and $E^Q_{cons.}$ have been reduced by 3.28% and 10.69% respectively. E^P_{loss} and E^Q_{loss} have been reduced by 9.54% and 9.9% respectively.

Table 2.3: Simulation results of TS-1 and TS-2 under TVVC and four Scenarios

Test system	Test system-1					Test system-2				
Scenarios	TVVC	SC-1	SC-2	SC-3	SC-4	TVVC	SC-1	SC-2	SC-3	SC-4
E^S_{demand}(MVAh)	88.372	84.368	83.672	83.323	82.632	608.45	581.56	580.44	546.06	542.44
ΔE^S_{demand}(MVAh)	——	4.004	4.7	5.049	5.74	——	26.89	28.01	62.39	66.01
ΔE^S_{demand}(%)	——-	4.53	5.32	5.71	6.49	——	4.42	4.6	10.25	10.84
$E^P_{cons.}$(MWh)	73.816	71.70	71.39	71.25	70.93	462.83	451.17	450.83	436.62	435.3
$\Delta E^P_{cons.}$(%)	——	2.866	3.28	3.47	3.9	——-	2.58	2.66	5.80	6.10
$E^Q_{cons.}$(MVARh)	44.590	40.27	39.82	39.67	39.18	370.64	342.24	341.07	307.82	304.54
$\Delta E^Q_{cons.}$(%)	——	9.68	10.69	11.03	12.13	——-	7.66	7.98	16.95	17.83
E^P_{loss}(MWh)	1.770	1.770	1.601	1.423	1.279	12.68	12.46	12.38	9.40	8.92
ΔE^P_{loss} (%)	———	0	9.54	19.6	27.74	——-	1.73	2.36	25.86	29.65
E^Q_{loss}(MVARh)	1.192	1.192	1.074	1.059	0.962	8.92	8.83	8.70	7.21	6.75
ΔE^Q_{loss}(%)	——	0	9.9	11.15	19.3	——	1	2.46	19.17	24.32
min. voltage (pu)	0.958	0.95	0.95	0.95	0.95	0.957	0.95	0.95	0.95	0.95
max. voltage (pu)	1.0125	1.016	1.007	1.001	0.994	1.05	1.041	1.040	1.004	1.00

Table 2.4: optimal opened RCS of TS-1 and TS-2 under Scenario 3 and Scenario 4

Hour duration	Opened RCS of TS-1				Opened RCS of TS-2			
	Scenario 3	N^S	Scenario 4	N^S	Scenario 3	N^S	Scenario 4	N^S
00:00 to 07:00	(7), (9), (14), (32), (37)	8	(6), (9), (13), (32), (37)	8	(23), (26), (48), (34), (45), (40), (58), (125), (95), (97), (71), (74), (130), (131), (109)	24	(21), (25), (48), (32), (45), (40), (60), (125), (95), (97), (70), (73), (130), (131), (132)	26
07:00 to 19:00	(7), (10), (14), (32), (37)	2	(7), (9), (13), (28), (37)	4	(23), (25), (50), (34), (44), (42), (61), (125), (95), (97), (71), (74), (130), (131), (109)	10	(21), (26), (48), (34), (45), (40), (58), (125), (95), (97), (71), (74), (130), (131), (109)	12
19:00 to 00:00	(7), (10), (14), (28), (32)	4	(6), (11), (14), (28), (37)	6	(23), (25), (50), (34), (44), (42), (61), (125), (95), (97), (71), (74), (130), (107), (132)	4	(21), (26), (50), (34), (45), (40), (58), (125), (95), (97), (71), (74), (130), (131), (132)	4
total N^S		14		18		38		42

(b) TS-2: $E^S_{demand.}$ has been reduced by 4.6%. $E^P_{cons.}$ and $E^Q_{cons.}$ have been reduced by 2.66% and 7.98% respectively. E^P_{loss} and E^Q_{loss} have been reduced by 2.36% and 2.46% respectively.

Thus, scenario 2, optimal operation of VVC devices with association of PVSI capable to reduce the E^S_{demand} upto 5.32% and 4.6% in TS-1 and TS-2 respectively.

2.5.2.3 Scenario 3

Under this scenario, it is assumed that PVSI is operated at unity power factor mode, whereas DNR operation, OLTC taps and SCBs operation remains active. Status of opened RCS over a day have been shown in Table 2.4 under scenario 3 for both TS.
(a)TS-1: E^S_{demand} has been reduced by 5.71%. $E^P_{cons.}$ and $E^Q_{cons.}$ have been reduced by 3.47% and 11.03% respectively. E^P_{loss} and E^Q_{loss} have been reduced by 19.6% and 11.15% respectively. The total N^S is noted as 14.
(b) TS-2: E^S_{demand} has been reduced by 10.25%. $E^P_{cons.}$ and $E^Q_{cons.}$ have been reduced by 5.8% and 16.95% respectively. E^P_{loss} and E^Q_{loss} have been reduced by 25.86% and l 19.17% respectively. The total N^S is noted as 38.
Thus, the application of optimal operation of VVC devices with association of DNR can reduce the E^S_{demand} upto 5.71% and 10.25% in TS-1 and TS-2 respectively.

2.5.2.4 Scenario 4

Under this scenario, it is assumed that PVSI is operated at Volt-VAR control mode. whereas DNR operation, OLTC taps and SCBs operation remains active. Status of opened RCS over a day have been shown in Table 2.4 under scenario 3 for both TS.
(a)TS-1: E^S_{demand} has been reduced by 6.49%. $E^P_{cons.}$ and $E^Q_{cons.}$ have been reduced by 3.9% and 12.13% respectively. The E^P_{loss} and E^Q_{loss} have been reduced by 27.74% and 19.3% respectively. The total N^S is 18.
(b) TS-2: $E^S_{demand.}$ has been reduced by 10.84%. $E^P_{cons.}$ and $E^Q_{cons.}$ have been reduced by 6.10% and 17.83% respectively. E^P_{loss} and E^Q_{loss} have been reduced by 29.65% and 24.32% respectively . The total N^S is 42.

Thus, combined operation of VVC devices, PVSI and DNR can efficiently reduce the E^S_{demand} upto 6.49% and 10.84% TS-1 and TS-2 respectively.

2.5.2.5 Voltage behavior at valley and peak loading hour for different scenarios

The valley and peak loads are observed at 04:00 and 19:00 from Fig.2.5. The voltage behaviour of the system for different scenarios have been drawn in Fig.2.8 and Fig.2.9 for TS-1 and TS-2 respectively. Fig.2.8a and Fig.2.9a presents the voltage behaviour of the

system observed at various buses at valley loading condition for TS-1 and TS-2 respectively. It can be observed that at valley loading hour, in TVVC method, the voltage at all nodes higher than the other scenarios. This indicates higher energy consumption under TVVC compared to other scenarios. This happens because increase in voltage would cause increase in energy consumption due to dependency of loads on voltage. However, scenario 1 to scenario 4, the voltage at all nodes have been observed closer to the lower portion of permissible limits, due to the optimal operation of control devices.

Similarly study is observed in the voltage behaviour of the system at peak loading condi-

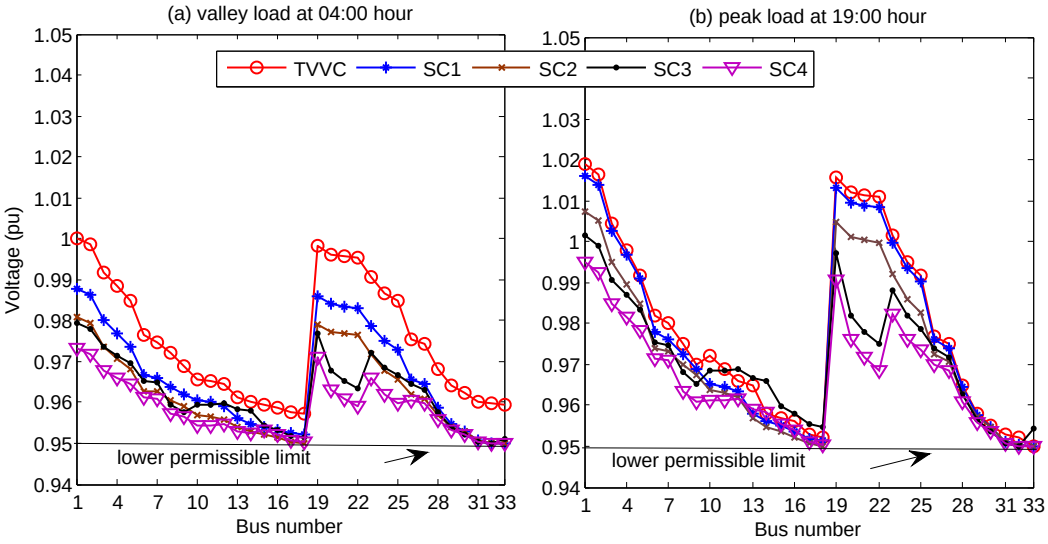

Figure 2.8: Voltage profile of TS-1 at (a)valley and (b)peak loading hour

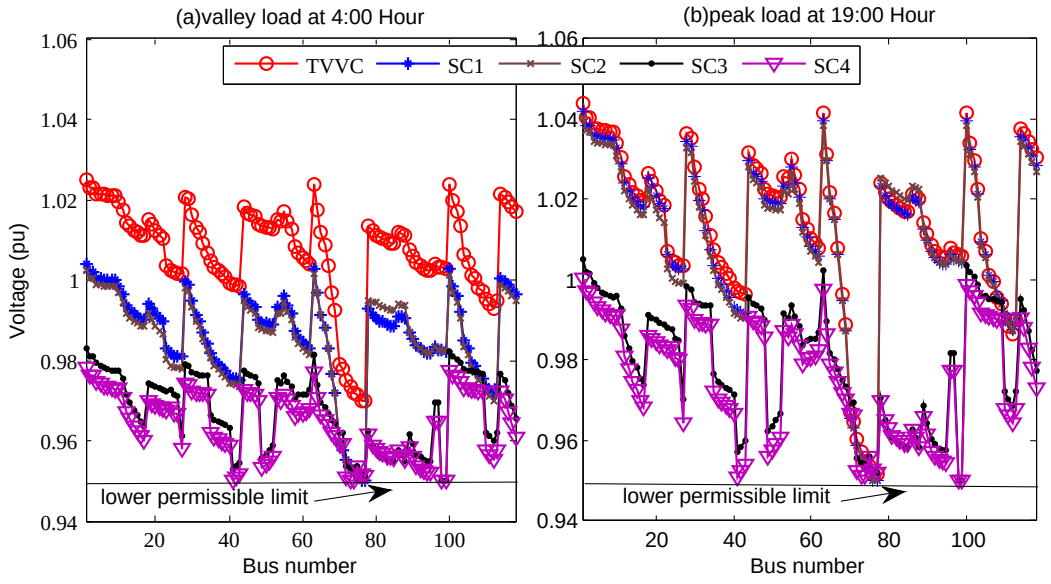

Figure 2.9: Voltage profile of TS-2 at (a) valley and (b) peak loading hour

tion as seen in Fig.2.8b and Fig.2.9b for TS-1 and TS-2 respectively. Thus, with optimal and coordinated operation of control devices, voltages at all nodes have been maintained closer to lower portion of permissible limit.

Under peak and valley loading hours, among all scenarios, scenario 4 (i.e. combined application of VVC devices, PVSI and DNR) has been found to be most effective to maintain the voltages just above the lower portion of permissible limits, which leads to maximum reduction of energy consumption.

2.5.2.6 Performance of MBGWO algorithm and other algorithms

Three major factors describes the capability of a metaheuristic algorithm [125]. (i) algorithms quality: best obtained solution (ii) algorithms robustness: standard deviation of the best solution among runs and (iii) effective runtime: defined as the average time to converge. The effective runtime T_c can be calculated by using (2.29)

$$T_c = \frac{iter^{con}}{iter^{\max}} T_{avg} \tag{2.29}$$

The performance of MBGWO algorithm for both TS-1 and TS-2 have been compared with the metaheuristic algorithms such as PSO, and conventional GWO (CGWO) for scenario 4 at peak loading hour (Hour-19:00). For all algorithms, same number of initial population (i.e 25), maximum iterations (i.e 100) and number of runs (i.e.20) have been taken. The convergence pattern of all algorithms have been plotted in Fig.2.10 for both TS. Further, capability parameters of all algorithms have been tabulated in Table 2.5 for both TS.

To begin with quality of the algorithm, proposed MBGWO algorithm has achieved minimum energy demand (i.e. 4.202 MVA for TS-1 and 27.55 MVA for TS-2), it can be found in Table 2.5. On the other hand, PSO algorithm settled next to MBGWO, whereas CGWO stands at third position. Moving on robustness, MBGWO comes with minimum standard deviation (i.e. 0.0317 MVA for TS-1 and 1.08 MVA for TS-2). As for PSO is preceding to the CGWO. Lastly, moving on to effective runtime, the MBGWO converges in less time (i.e. 2.541 sec. for TS-1 and 5.415 sec. for TS-2) compared with other algorithms.

Therefore, modifications in wolf position update mechanism using (2.23)-(2.26) is helpful for MBGWO algorithm to yields better results in aforementioned capability factors

Table 2.5: Performance of various algorithms for Scenario 4 at peak loading hour for TS-1 and TS-2

Test system	TS-1			TS-2		
Algorithm	CGWO	PSO	MBGWO	CGWO	PSO	MBGWO
Best (MVA)	4.29	4.26	4.202	28.6	28.2	27.55
Average (MVA)	4.31	4.292	4.208	29.59	29.45	27.89
Worst (MVA)	5.23	5.02	4.4	46.52	46.23	34.2
Std. deviation (MVA)	0.110	0.103	0.0317	2.81	3.32	1.08
$iter^{con}$	12	11	7	20	22	12
T_c (sec.)	4.8	5.005	2.541	9.586	9.937	5.415
T_{avg} (sec.)	40.02	45.5	36.3	47.93	52.3	45.13

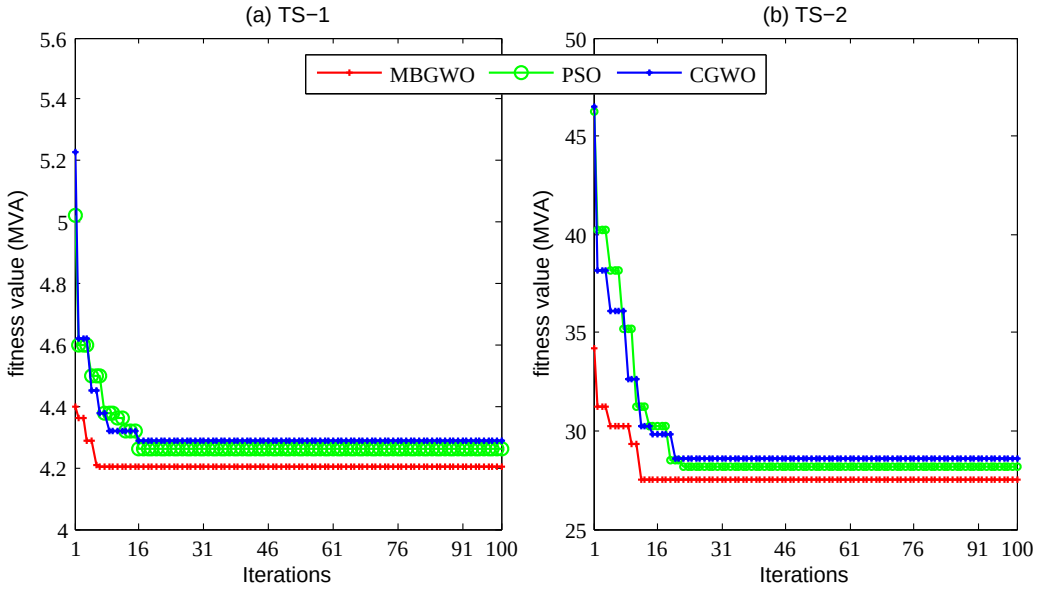

Figure 2.10: Convergence curve of different algorithms of (a)TS-1 and (b)TS-2 under scenario 4, at peak hour (19:00)

than the PSO and CGWO algorithms.

Besides, the present non-convex MINLP problem has been solved using Discrete and continuous optimizer (DICOPT) solver in general algebraic modeling system (GAMS) platform [134] . In DICOPT solver, a MINLP problem has been solved by a series of NLP (nonlinear programming) and MIP (mixed integer programming) sub problems. Table 2.6 shows the performance of MBGWO and DICOPT solver for scenario 4 at peak loading hour (i.e. 19:00 hour) for TS-1 and TS-2. It can be observed that the proposed MBGWO algorithm is able to produce a better solution compared with DICOPT. Concerning the

computational effort, both proposed MBGWO and DICOPT have convergence almost same time. But, DICOPT gets trapped in local minimum due to complex and non-convex nature of present MINLP problem.

From the above analysis, it can be concluded that the proposed MBGWO algorithm performs better than the other methods such as PSO, CGWO and DICOPT solver. Therefore, proposed MBGWO can be suggested for solving the present complex and non-convex MINLP problem.

Table 2.6: Performance of MBGWO and DICOPT for Scenario 4 at peak loading hour for TS-1 and TS-2

Test systems	TS-1		TS-2	
Algorithms	MBGWO	DICOPT [134]	MBGWO	DICOPT [134]
Objective function (MVA)	4.202	4.24	27.55	28.02
T_c (sec.)	2.541	2.54	5.415	5.4

2.5.2.7 33 bus unbalanced distribution system

The performance of the control scheme has been tested on unbalanced IEEE 33-bus distribution system using OpenDSS COM interface with MATLAB [135]. Fig. 2.11 depicts the single diagram of unbalanced IEEE 33-bus distribution system. The methodology has been developed in MATLAB, while power flow has been solved in OpenDSS. The detailed unbalanced load data and line data has been taken from [136]. The nominal voltage of the system is 12.66 kV. The total nominal real and reactive power loads on the system are 3.635 MW and 2.265 MVAR respectively. The OLTC of the three-phase substation transformer in branch 1-2 has 5 steps enabling a ±5% turn ratio change. SCBs are installed at buses 14 and 26. Each has a capacity of 180 kVAR per phase; Four PV smart inverters each with the capacity of 300 kVA are installed at buses 10, 17, 22, and 32 respectively, where PV-1 is three-phase integrated, PV- 3 is AB-phase integrated, PV-2 and PV-4 are just A-phase integrated. The permissible system voltage limits of 0.95 to 1.05 pu have been chosen.The simulation results of unbalanced 33 bus distribution system under TVVC and four scenarios have been tabulated in Table 2.7 for exponential load models (ELM).

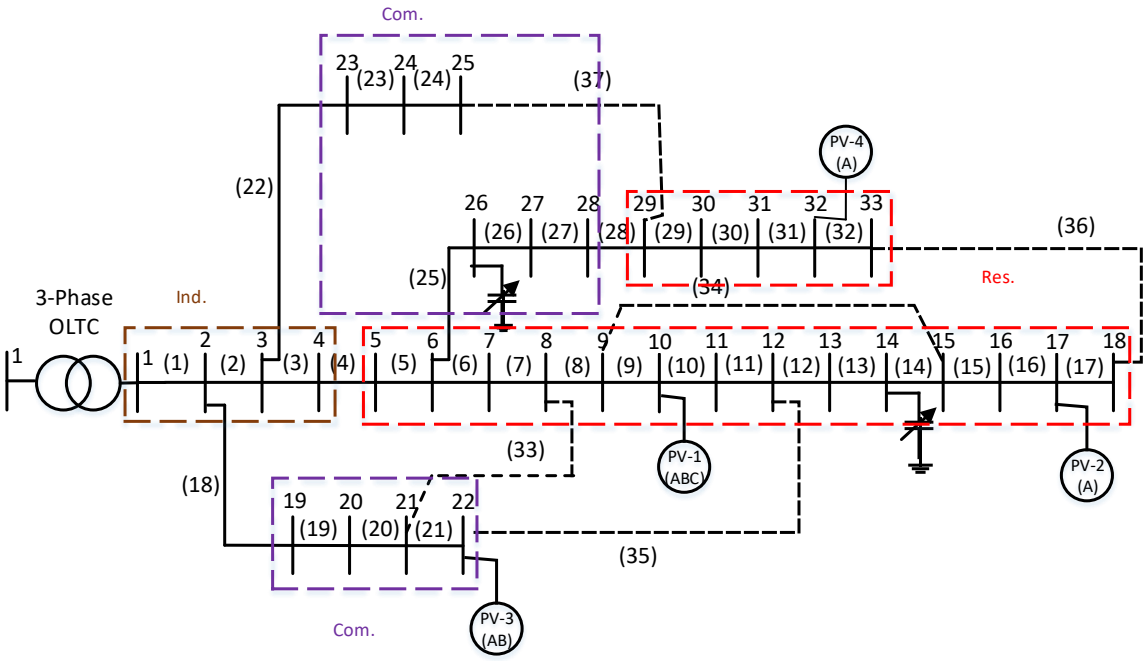

Figure 2.11: modified unbalanced 33 bus distribution system

Table 2.7 shows that compared with TVVC, the E^S_{demand} of the system has been reduced by 6.105% with optimal operation of VVC devices as seen in scenario 1. Further 0.146% more reduction in E^S_{demand} has been achieved with the active participation of reactive power dispatch from smart inverter as seen in scenario 2. With combined operation of DNR and VVC devices, E^S_{demand} of the system has reduced by 6.506% as seen in scenario 3, further 0.118% more reduction in E^S_{demand} has been achieved with the active participation of reactive power dispatch from smart inverter as seen in scenario 4.Thus, coordinated operation of DNR, VVC devices and smart inverter leads to fruitful results even in unbalanced distribution system.

2.5.2.8 Impact of forecast error

In reality, the PV generation output and the load of any particular day have some forecasting error. Stochastic analysis has been applied to consider the impact of forecast error on the results of the optimization problem. Here, the standard deviation of the forecasted PV output and load have been taken as $\pm 15\%$ and $\pm 10\%$ of their mean value respectively for each hour. A Gaussian distribution has been employed to simulate the PV output and the load demand. Further, the Monte Carlo simulation has been performed with 500 scenarios. In order to reduce the computational burden, scenarios have been reduced to

Table 2.7: Simulation results of unbalanced 33 bus distribution system under TVVC and four Scenarios

Scenarios		TVVC	SC-1	SC-2	SC-3	SC-4
E^S_{demand} (MVAh)	A phase	27.858	25.964	25.854	25.892	25.797
	B phase	27.962	26.346	26.334	26.210	26.204
	C phase	28.498	26.860	26.856	26.730	26.731
	total	84.318	79.170	79.044	78.832	78.732
ΔE^S_{demand}(MVAh)		—-	5.148	5.274	5.486	5.586
ΔE^S_{demand} (%)		—-	6.105	6.254	6.506	6.624
$E^P_{cons.}$ (MWh)		71.491	68.823	68.739	68.682	68.625
$\Delta E^P_{cons.}$ (%)		—-	3.731	3.849	3.929	4.00
$E^Q_{cons.}$ (MVARh)		42.842	37.637	37.517	37.467	37.368
$\Delta E^Q_{cons.}$ (%)		—-	12.149	12.429	12.546	12.77
E^P_{loss}(MWh)		0.810	0.605	0.609	0.483	0.480
ΔE^P_{loss} (%)		—-	25.30	24.81	40.30	40.74
E^Q_{loss} (MVARh)		0.542	0.411	0.416	0.359	0.359
ΔE^Q_{loss} (%)		—-	24.169	23.24	33.763	33.763

15 scenarios by using k-means clustering [137].

Fig.2.12 represents the E^S_{demand}, $E^S_{savings}$ and lowest voltage of the system at each hour obtained with consideration of forecasted error under TVVC and scenario 4. It can be observed that significant $E^S_{savings}$ have been achieved, while maintaining the volatge above lower permissible limit (i.e. 0.95pu) as seen in Fig.2.12c and Fig.2.12d respectively at each hour.

Thus, it can be concluded that the control setting obtained by proposed scheme is effective even in the occurrence of forecast errors within the above mentioned range.

2.5.3 Effect of different load models under different scenarios

In this section, MBGWO algorithm has been employed on exponential and ZIP loads models for energy demand reduction under four scenarios. Fig.2.13 and Fig.2.14 portray the percentage reduction of energy terms under four scenarios with respect to the TVVC for TS-1 and TS-2 respectively.

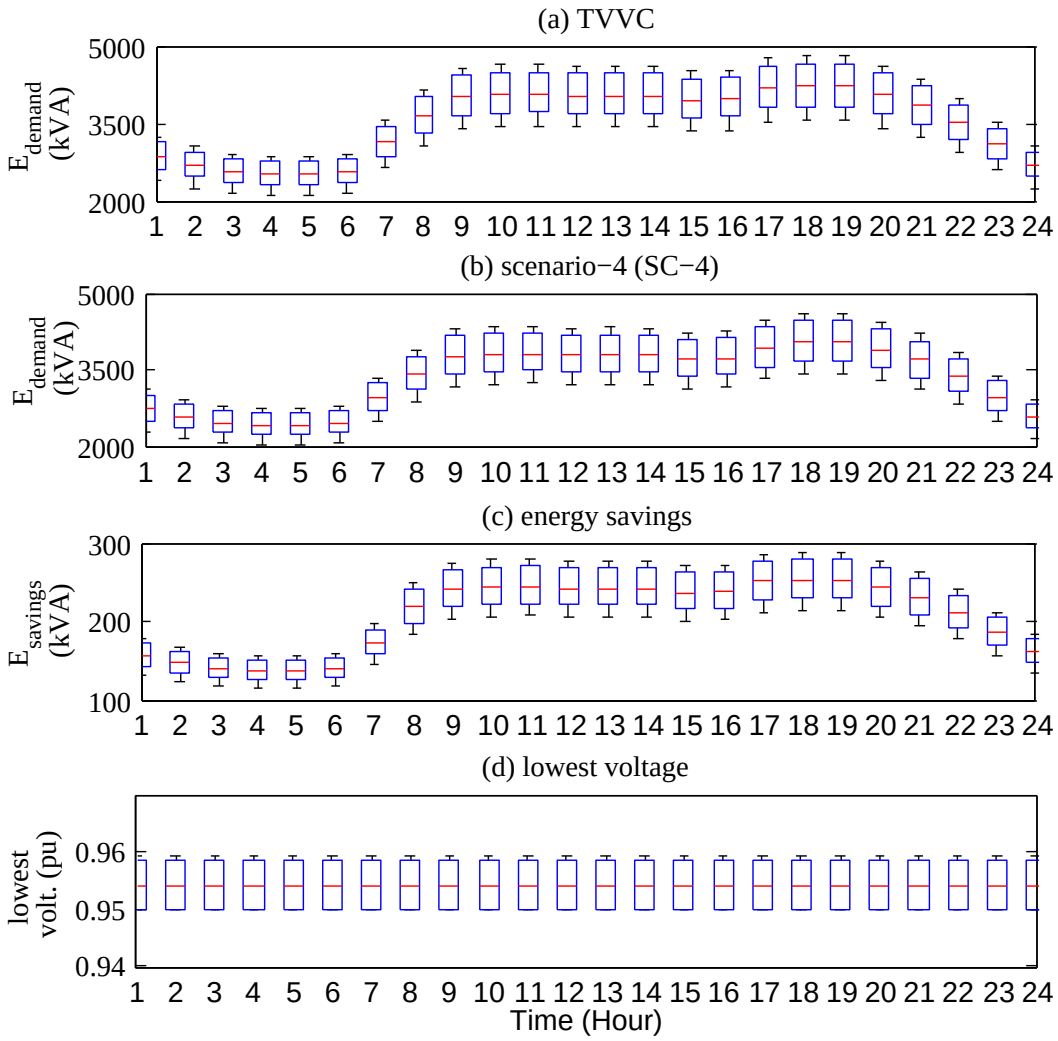

Figure 2.12: Stochastic analysis: forecasted errors for unbalanced 33 bus system

TS-1: From Fig.2.13, it can be observed that under scenario 2 percentage E^S_{demand} reduction is 0.79% (i.e. $5.32\% - 4.53\% = 0.79\%$) more for ELM and 0.5% (i.e. $4.8\% - 4.3\% = 0.5\%$) for ZIP than scenario 1. This is due to coordinated operation of VVC devices and PVSI. Under scenario 3, optimal coordination of VVC devices and DNR yields 0.39% for ELM and 0.21% for ZIP more E^S_{demand} reduction than scenario 2. under scenario 4, percentage E^S_{demand} reduction is 0.78% more for ELM and 0.5% for ZIP than scenario 3. This is due to the coordinated operation of all the control devices (VVC devices, PVSI and DNR).

TS-2: From Fig.2.14, it can be observed that under scenario 2, percentage E^S_{demand} reduction is 0.18% more for ELM and 0.14% for ZIP than scenario 1. This is due to coordinated operation of VVC devices and PVSI. Under scenario 3, optimal coordination of VVC de-

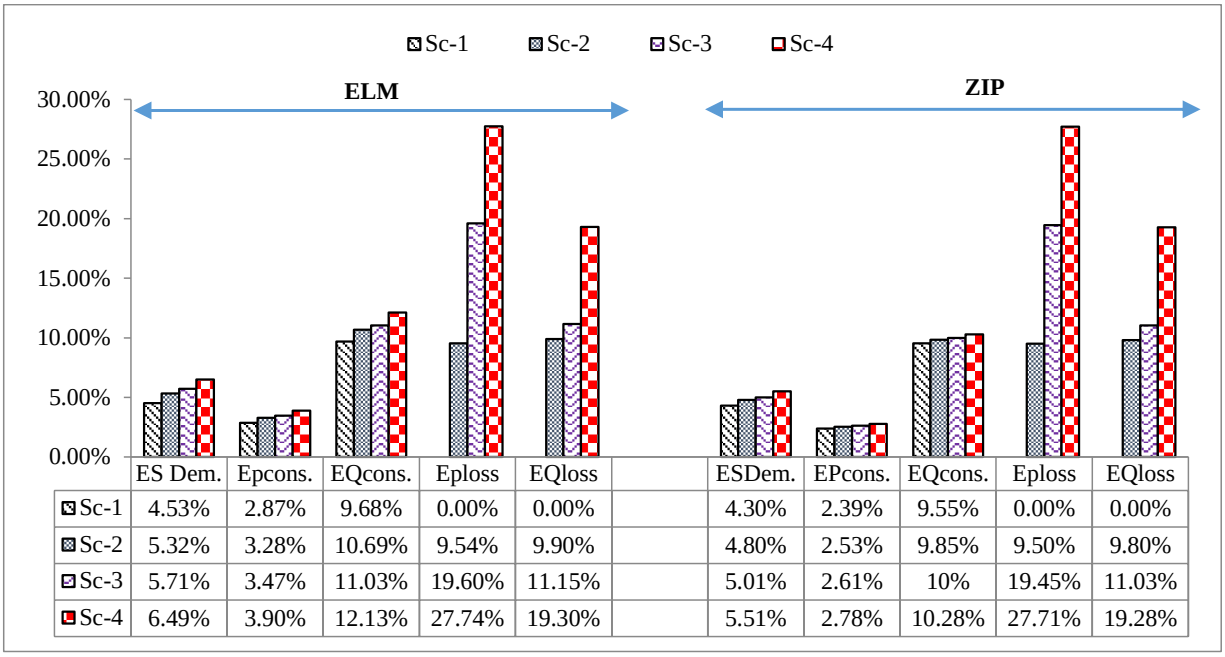

	ES Dem.	Epcons.	EQcons.	Eploss	EQloss		ESDem.	EPcons.	EQcons.	Eploss	EQloss
Sc-1	4.53%	2.87%	9.68%	0.00%	0.00%		4.30%	2.39%	9.55%	0.00%	0.00%
Sc-2	5.32%	3.28%	10.69%	9.54%	9.90%		4.80%	2.53%	9.85%	9.50%	9.80%
Sc-3	5.71%	3.47%	11.03%	19.60%	11.15%		5.01%	2.61%	10%	19.45%	11.03%
Sc-4	6.49%	3.90%	12.13%	27.74%	19.30%		5.51%	2.78%	10.28%	27.71%	19.28%

Figure 2.13: Percentage energy reduction in ELM and ZIP load models of TS-1 under four scenarios compared with TVVC

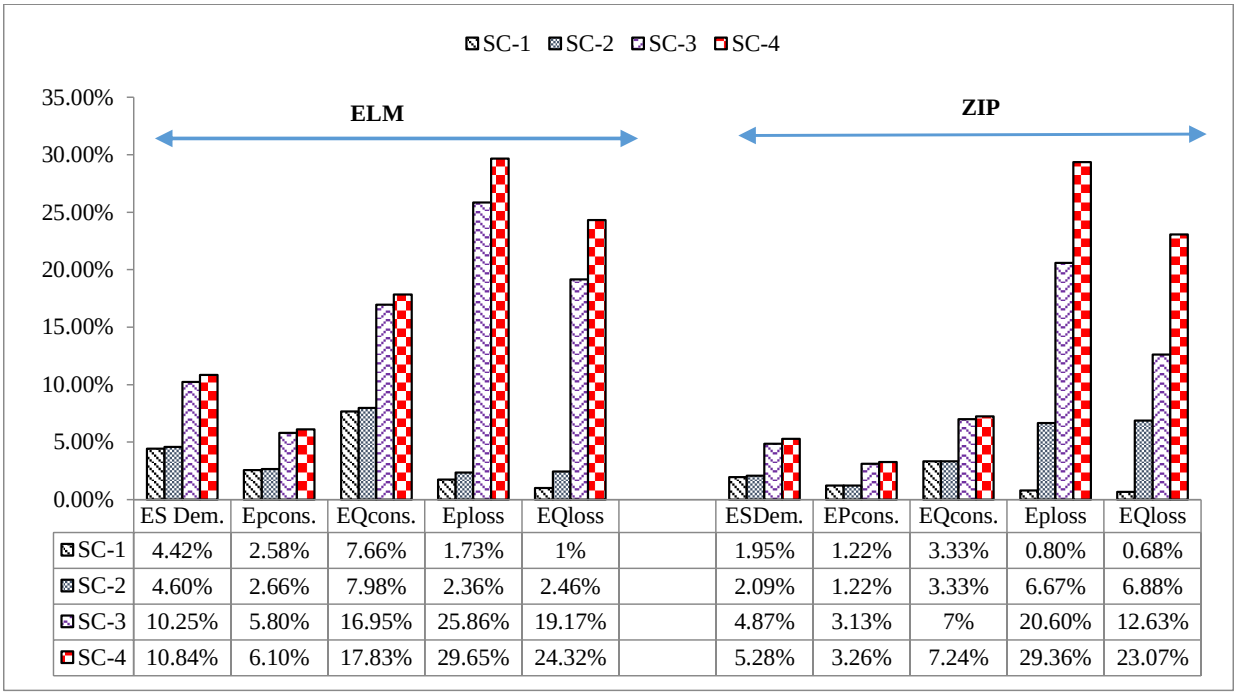

	ES Dem.	Epcons.	EQcons.	Eploss	EQloss		ESDem.	EPcons.	EQcons.	Eploss	EQloss
SC-1	4.42%	2.58%	7.66%	1.73%	1%		1.95%	1.22%	3.33%	0.80%	0.68%
SC-2	4.60%	2.66%	7.98%	2.36%	2.46%		2.09%	1.22%	3.33%	6.67%	6.88%
SC-3	10.25%	5.80%	16.95%	25.86%	19.17%		4.87%	3.13%	7%	20.60%	12.63%
SC-4	10.84%	6.10%	17.83%	29.65%	24.32%		5.28%	3.26%	7.24%	29.36%	23.07%

Figure 2.14: Percentage energy reduction in ELM and ZIP load models of TS-2 under four scenarios compared with TVVC

vices and DNR yields 5.65% for ELM and 2.78% for ZIP more E^S_{demand} reduction than scenario 2. under scenario 4, percentage E^S_{demand} reduction is 0.59% more for ELM and 0.41% for ZIP than scenario 3. This is due to the coordinative operation of all the control devices.

Thus, proper coordination of control devices can yield higher E^S_{demand} reduction in both ELM and ZIP load model in both TS. With reference to above study, it is also observed that percentage E^S_{demand} reduction in ELM is more than ZIP load model.

2.5.4 Service restoration considering voltage regulation and peak demand reduction

In this study, proposed algorithm (Algorithm 2) has been implemented for the service restoration considering voltage regulation and peak demand reduction under faulty condition.

In order to show the impact of combined operation of VVC devices and PVSI, three different cases have been studied under proposed method for exponential load model (ELM), namely

- case 1: load restoration only (i.e. disabled VVC devices and PVSI is operated at unity power factor) considering faulty condition
- case 2: load restoration, enabled VVC devices and PVSI is operated at unity power factor considering faulty condition
- case 3: load restoration, enabled VVC devices and PVSI is operated at non-unity power factor considering faulty condition

Multiple line faults have been considered for analysis in both TS. Table 2.8 depicts the summary of results under peak demand (i.e. 1.0 pu). Fig.2.15 show the bus voltage profile at faulty condition and three cases for both TS.

TS-1: Assume that fault has taken place at three locations i.e. branch 5, 21, 26. At faulty state, bus 6 to 18, bus 21 and bus 26 to 33 are deprived of supply as seen in Fig.2.15a. In case 1, 100% loads have been recovered by closing RCS 33, 35, and 37. But the voltage at bus 9 to 17 and bus 22 violates the lower permissible limit (i.e. 0.95 pu) as seen in

Fig.2.15a. The minimum voltage is equal to 0.925 found at bus 18. Whereas, case 2 and case 3, 100% loads have been recovered by closing RCS 33, 35, and 37. Besides, the minimum voltage was obtained as 0.953 pu at bus 18 and 0.95 pu at bus 33 in case 2 and case 3 respectively, with the support of VVC devices and reactive power from PVSI. Among case 2 and case 3, case 3 achieves 1.28% more power demand ($S_{dem.}$) reduction than case 2. This is because of reactive power Q_{inv} support provided by the PVSI, which can seen in Table 2.8 under TS-1.

TS-2: Assume that fault has occurred at three locations i.e. branch 22, 70, and 106.

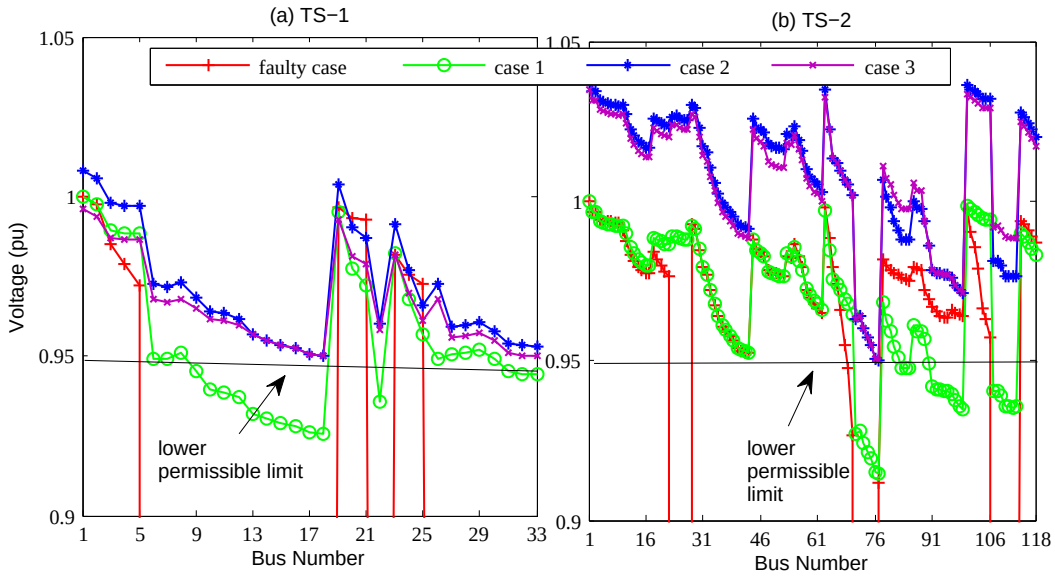

Figure 2.15: Voltage profile of TS-1 and TS-2 under different cases

Under faulty state, bus 23 to 27, bus 71 to 76 and bus 107 to 113 have been deprived service as seen in Fig.2.15b. In case 1, 100% loads have been recovered by closing RCS 118, 128, and 131. But the voltage at bus 71 to 76, bus 91 to 99 and bus 107 to 113 violates the lower permissible limit as seen in Fig.2.15b. The minimum voltage is equal to 0.914 found at bus 77. Whereas in case 2 and case 3, 100% loads have been recovered by closing RCS 118, 128, and 131. Further, the lower voltage has maintained within permissible limits. From Table 2.8, it can be observed that case 3 achieves 0.353% more power demand ($S_{dem.}$) reduction than case 2. This is due to the Q_{inv} support provided by the PVSI.

Table 2.8: simulations results of TS-1 and TS-2 under multiple line faults at peak demand

parameters	TS-1			TS-2		
cases	case 1	case 2	case 3	case 1	case 2	case 3
fault location	(5), (21) & (26)			(22), (70) & (106)		
opened switches	(5) (21) & (26)			(22), (70) & (106)		
closed switches	(33) (35) & (37)			(118),(128) & (131)		
load restoration (%)	100	100	100	100	100	100
min. volt. (pu)	0.925	0.953	0.95	0.914	0.956	0.95
max. volt. (pu)	1	1.007	0.996	1	1.037	1.035
P_{loss}(MW)	0.146	0.134	0.119	0.744	0.719	0.689
ΔP_{loss} (%)	——	——	11.19	——	—-	4.17
Q_{loss} (MVAR)	0.115	0.106	0.096	0.521	0.533	0.499
ΔQ_{loss} (%)	——-	——-	9.43	——-	——-	6.37
$P_{cons.}$ (MW)	3.523	3.582	3.562	21.715	22.715	22.700
$\Delta P_{cons.}$ (%)	——-	——-	0.56	——-	——-	0.066
$Q_{cons.}$ (MVAR)	1.919	2.023	1.983	15.105	17.652	17.571
$\Delta Q_{cons.}$ (%)	——-	——-	1.97	——-	——-	0.458
$S_{dem.}$(MVA)	4.198	4.286	4.231	27.360	29.663	29.558
$\Delta S_{dem.}$ (%)	——-	——-	1.28	——-	——-	0.353
OLTC tap	0	+1	+1	0	+6	+6
four SCBs step	0,0,0,0	2,2,2,2	2,2,2,2	0,0,0,0	4,4,4,4	4,4,4,4
Q_{pv}^{inv*} (MVAR)	—-	—-	1.05	—-	—-	3.82

*indicates aggregate value

2.5.5 Performance of proposed algorithm with association of PVSI droop control considering cloudy condition

The typical PV output profile shown in Fig.2.5 is valid for a clear sky day. However, in reality many days are fully cloud and partly cloud days. Power fluctuation may exist in the system, when a cloud is passing over the high penetrated PV installed distribution network.

For illustration, it is assumed that partly clouds and fully clouds occurred between

Table 2.9: PV output during clear sky, partly and fully cloud day condition

Time (HH:MM)	13:00	13:15	13:30	13:45	14:00
PV output (p.u) @ clear sky	0.9	0.89	0.88	0.87	0.85
PV output (p.u) @ cloudy	0.9	0.667 (25% reduction)	0.44 (50% reduction)	0 (100% reduction)	0.85

13:00 to 14:00 hours for both TS. A sudden change in PV generation output depicted in Table 2.9, at hour 13:15, 13:30, and 13:45, PV output has been reduced by 25%, 50% and 100% from the normal clear sky condition due to partly cloud and full cloud condition respectively.

In clear cloud day, using MBGWO algorithm (algorithm 1), settings of control parameters such as OLTC tap position, SCBs, and opened RCS were obtained and depicted in Table 2.10 for both TS during 13:00 to 14:00 hour having load of 0.95 pu considering exponential load model (ELM). At hour 13:00, lowest voltage of the system is at 0.956 pu for TS-1 and

Table 2.10: Status of VVC devices, DNR and PVSI reactive power using proposed algorithm during 13:00 to 14:00 hours

Test system	Time duration	OLTC tap	Q^{SCB^*} (MVAR)	Opened RCS	$Q_{pv}^{inv^*}$ (MVAR)
TS-1	13:00 to 14:00	-2	1.2	(7), (10), (14), (32), (37)	0.504
TS-2	13:00 to 14:00	-1	2.4	(21),(26),(48), (34),(45), (40),(58),(125), (95),(97), (71), (74),(130),(131), (109)	1.74

* indicates aggregate value

0.954 pu for TS-2, Similarly at hour 14:00, lowest voltage of the system is at 0.954 pu for TS-1 and 0.952 pu for TS-2, which are in dead band range of PVSI droop characteristics.

At these time instants, PVSI neither inject nor absorbs the additional reactive power. Therefore, reactive power of PVSI at this instant is same as their previous settings (as determined in normal clear day). Under the partly and cloudy days, lowest voltage of the system fall below point V_2 (i.e. 0.95 pu) from hour 13:15 to 13:45, which can be seen in Table 2.11 and Table 2.12 for TS-1 and TS-2 under no control. This is due to reduction of PV active power output under cloudy condition.

Under this circumstances, the proposed algorithm with association of PVSI droop control has been utilised as discussed in algorithm 3. The droop parameter setting is given in Appendix A.1. In time duration 13:15 to 13:45 hours, PVSI can provide the additional reactive power support, since the active power output is less than rated capacity of the PVSI. At 13:15 hour, with the support of available reactive power of PVSI as governed by (27), the lowest voltage of the system brought to above lower permissible limit (i.e. 0.95 pu) for both TS. However, at 13:30 and 13:45 hours, available reactive power of PVSI cannot restore the voltage due to high reduction of PV generation, in such case reschedule the settings of VVC devices, PVSI and status of RCS using MBGWO algorithm for both TS, then the lowest voltage of the TS brought to above lower permissible limit as seen in Table 2.11 and Table 2.12 for TS-1 and TS-2 respectively under proposed algorithm with PVSI droop control. Subsequently power losses has been reduced. However, energy consumption of load has been increased due to increase in voltages.

The sudden disappearance of cloud or reduction in load demand may result in voltage rise problem. In this situation, the voltage rise can be controlled by absorbing the reactive power through PVSI based on droop controller. In case voltage is still violating the permissible limit, after full utilization of PVSI. The operator has to be reschedule the control devices such as VVC devices and RCS.

Table 2.11: Summary of results during clear sky, partly and full cloudy condition for TS-1

Time (HH:MM)	$P_{pv}^{inv^*}$ (MW)	No control (previous setting)					Proposed algorithm with PVSI droop control						
		$P_{cons.}^{*}$ (MW)	$Q_{cons.}^{*}$ (MVAR)	P_{loss}^{*} (MW)	Q_{loss}^{*} (MVAR)	Min. Volt. (pu)	$Q_{pv}^{inv^*}$ (MVAR)	OLTC tap	$P_{cons.}^{*}$ (MW)	$Q_{cons.}^{*}$ (MVAR)	$P_{loss.}^{*}$ (MW)	Q_{loss}^{*} (MVAR)	Min. Volt. (pu)
13:00	1	3.429	1.906	0.054	0.04	0.956	0.504	-2	3.429	1.906	0.054	0.04	0.956
13:15	0.747	3.408	1.896	0.079	0.053	0.946	0.834	-2	3.413	1.911	0.06	0.041	0.951
13:30	0.492	3.39	1.85	0.096	0.067	0.942	0.98	-1	3.413	1.911	0.063	0.042	0.953
13:45	0	3.38	1.82	0.12	0.088	0.938	1.1	0	3.414	1.912	0.066	0.044	0.951
14:00	0.952	3.426	1.9	0.058	0.045	0.954	0.586	-2	3.426	1.9	0.058	0.045	0.954

* indicates aggregate value

Table 2.12: Summary of results during clear sky, partly and full cloudy condition for TS-2

Time (HH:MM)	P_{pv}^{inv*} (MW)	No control (previous setting)					Proposed algorithm with PVSI droop control						
		$P^*_{cons.}$ (MW)	$Q^*_{cons.}$ (MVAR)	P^*_{loss} (MW)	Q^*_{loss} (MVAR)	Min. Volt. (pu)	Q_{pv}^{inv*} (MVAR)	OLTC tap	$P^*_{cons.}$ (MW)	$Q^*_{cons.}$ (MVAR)	$P^*_{loss.}$ (MW)	Q^*_{loss} (MVAR)	Min. Volt. (pu)
13:00	3.6	20.91	14.89	0.36	0.27	0.954	1.74	-1	20.91	14.89	0.36	0.27	0.954
13:15	2.67	20.73	14.51	0.44	0.337	0.944	2.978	-1	20.9	14.87	0.375	0.287	0.956
13:30	1.76	20.73	14.5	0.48	0.355	0.94	3.6	0	20.89	14.86	0.38	0.291	0.951
13:45	0	20.69	14.32	0.562	0.402	0.936	3.9	1	20.89	14.84	0.386	0.295	0.95
14:00	3.4	20.89	14.86	0.38	0.28	0.952	2.107	-1	20.89	14.86	0.38	0.28	0.952

* indicates aggregate value

2.6 Conclusion

An efficient and optimally coordinated operation of VVC devices, PVSI and DNR for energy savings has been presented. Test results of TS-1 and TS-2 have been reported as corroborative evidence of proposed method, which reveals that

- Optimally coordinated operation of VVC devices, PVSI and DNR can yield upto 6.49% and 10.84% more energy savings in TS-1 and TS-2, respectively, compared with the traditional VVC technique.
- A Significant amount of energy savings can be achieved by the proposed method in both exponential and ZIP load models.
- Under the faulty condition, the proposed method can effectively restore the l00% load while maintaining the voltage within permissible limits and also achieved peak demand reduction.
- The proposed method with an association of a PVSI droop control scheme can actively handle the voltage violations during partly and fully cloud conditions.
- The proposed method is effective even in the occurrence of forecasting errors in PV output and load.
- The performance of the proposed MBGWO algorithm is better than CGWO and PSO algorithms because it inherited the nature of both PSO and CGWO algorithms.

Chapter 3

Minimization of Operational Cost in Active Distribution System considering Network Reconfiguration and Soft Open Point

3.1 Introduction

Presently, electricity is a basic need for sustainable development of modern society. Therefore, energy demand has been increasing rapidly across the world. Conservation voltage reduction (CVR) is a promising technique utilized by distribution system operators (DSO) for peak demand reduction and energy savings in distribution system [60]. Traditionally, CVR operation has been conducted by OLTC transformer, switched capacitor banks (SCBs) and voltage regulator (VRs) for energy demand reduction. However, operation of these control devices is limited due to their physical constraints [138]. To cope up with increasing energy demand, existing network needs to be strengthened with the advanced operational tools in smart grid environment.

Distribution network reconfiguration (DNR) is an effective technique to improve the operation efficiency of distribution systems. Benefits of DNR operation in distribution system under different time zones has been conducted in [139]. On the other side, soft open points (SOP) are paying more attention due to flexibility of the power electronic devices in smart distribution system. SOP can provide active power flow control between the